molecular pharmaceutics

Article

pubs.acs.org/molecularpharmaceutics

Bioresorbable Polymer Coated Drug Eluting Stent: A Model Study

Filippo Rossi,[†] Tommaso Casalini,[†] Edoardo Raffa, Maurizio Masi, and Giuseppe Perale*

Department of Chemistry, Materials and Chemical Engineering "Giulio Natta", Politecnico di Milano, Via Mancinelli 7, 20131 Milano, Italy

ABSTRACT: In drug eluting stent technologies, an increased demand for better control, higher reliability, and enhanced performances of drug delivery systems emerged in the last years and thus offered the opportunity to introduce model-based approaches aimed to overcome the remarkable limits of trial-and-error methods. In this context a mathematical model was studied, based on detailed conservation equations and taking into account the main physical-chemical mechanisms involved in polymeric coating degradation, drug release, and restenosis inhibition. It allowed highlighting the interdependence between factors affecting each of these phenomena and, in particular, the influence of stent design parameters on drug antirestenotic efficacy. Therefore, the here-proposed model is aimed to simulate the diffusional release, for both in vitro and the in vivo conditions: results were verified against various literature data, confirming the reliability of the parameter estimation procedure. The hierarchical structure of this model also allows easily modifying the set of equations describing restenosis evolution to enhance model reliability and taking advantage of the deep understanding of physiological mechanisms governing the different stages of smooth muscle cell growth and proliferation. In addition, thanks to its simplicity and to the very low system requirements and central processing unit (CPU) time, our model allows obtaining immediate views of system behavior.

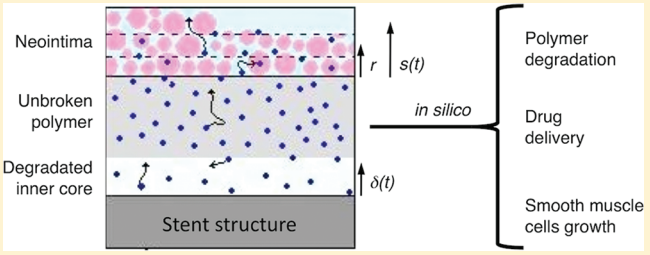

KEYWORDS: *stent, mathematical modeling, polymers, controlled drug delivery*

1. INTRODUCTION

Since the first polymer-based drug eluting stent (DES) was approved by US Food and Drug Administration (FDA), the Cypher stent, many other DES's have been studied worldwide.[1,2] Some trials and clinical outcomes showed encouraging *in vivo* results,[3] but worrying doubts and cautionary voices were raised from part of the scientific community too.[4−6] In particular, in the case of permanent-polymer based formulations, several studies showed the influence of polymer−tissue interactions that can induce severe host tissue responses, such as marked detrimental inflammatory responses or subacute thrombosis, even when high antirestenotic drug doses were delivered.[6−9] However, in the last year, some biodegradable-polymer based formulations, innovative coating techniques,[10,11] and new biological targeting methods[12,13] became altogether interesting, as far as they offer the opportunity to enhance the efficacy of local drug delivery against restenosis:[14,15] for instance, DES's coated with bioresorbable polymeric thin films were successfully implanted into the first patient in 2000.[16,17] Such new advances, coupled with a more reliable understanding of the mechanisms governing drug release and polymer degradation kinetics, may contribute to the development of a new generation of DES's.[18,19] However, as emerges from literature, reliable control on drug delivery and proper characterization of polymer−tissue interactions is not yet available for many of the biodegradable-polymer formulations used in DES technology. In particular, even if the "burst effect" seems to be avoided in some recent coating formulations,[10,20] the presence of long chain fragments, byproducts of polymer degradation, still strongly influences the ability to properly control drug delivery: this often leads to inadequate inhibition of undesired host tissue responses, such as incomplete healing or the late persistence of macrophages.[21,22]

Polymers may reduce undesired in-stent restenosis just after stent implantation, but available data often show low or even no accordance.[10,23−26] Indeed, the neointimal thickening may easily occur already few days after surgery, embedding the DES until a total occlusion of vessel lumen. In literature it is generally accepted that smooth muscle cells (SMC), normally present in a quiescent state in the media tissue, play a key role in the pathway of events that contribute to the formation of neointimal hyperplasia via long-term proliferation and migration.[24,27,28] In particular, within the 24 h following balloon catheter injury to arteries, the SMC start to replicate, and once they reach the intima, they can undergo a sustained replication for a period of several weeks until re-endothelialization events occur.[28] It is well-known[29] that neointimal tissue strongly affects drug distribution within the neointimal itself and the artery wall medial tissues and, hence, antirestenotic drug efficacy too.

In summary, the design of an effective DES requires a complex approach to optimize drug release profiles, coating degradation properties and restenosis inhibition. Mathematical

Received: November 11, 2011
Revised: May 10, 2012
Accepted: May 16, 2012
Published: May 16, 2012

 © 2012 American Chemical Society

modeling tools are surely appropriate to study all such phenomena together and to describe underlying physical mechanisms, encouraging researchers to avoid trial-and-error approaches toward rational model-based methods.[30,31] On the modeling side, literature offers a wide number of computational examples and mathematical models of different complexity. Finite element methods (FEM) represent the most common approach to solve systems of partial differential equations, which combine diffusion, mechanical behavior, and blood flow influence (through fluid dynamics models), to best capture the synergy of involved phenomena.[32] Moreover, such models can also be referred to complex geometries, that may also explicitly include an artery environment.[33,34] In the drug delivery field, models are usually aimed to describe release profiles,[35] taking into account drug distribution in arterial walls,[36−39] blood flow influence,[40−44] or coating degradation.[45] Stent mechanical analysis is aimed to study structural stresses[46] and may couple structure behavior with bloodstream,[47] stent expansion,[48] or coating degradation[49] effects; various approaches were proposed, as recently reviewed.[30]

Aiming to reach a decisive impact in the rational design of new biodegradable polymer-based DES, our attention was focused on the processes governing drug release. Indeed, the model considers at the same time polymer degradation, drug release, and SMC growth, capturing the synergic effects that occur among all of these phenomena. Several systems were analyzed to prove model reliability and hypothesis coherence by comparing simulation results with experimental data. Once model validation was achieved, it was then possible to evaluate the role played by polymer degradation kinetics and neointimal tissue growth on antirestenotic drug efficacy. In particular, data taken from literature consist of release studies for different drugs (paclitaxel, rapamycin, and heparin) from biodegradable aliphatic polyesters films, *in vitro* growth inhibition assays, and *in vivo* neointimal thickening. The wide spectrum of published experimental data here addressed is the following:

- *in vitro* hydrolytic degradation of thin (10 μm) and thick (100 μm) poly(lactic-*co*-glycolic acid) (PLGA) and polycaprolactone (PCL) films, molecular weight distributions during degradation times;[50,51]
- *in vitro* PLGA coated DES mass loss during degradation times;[52]
- *in vitro* paclitaxel release from thin (8 μm) PLGA coated DES;[53]
- *in vitro* paclitaxel release from thick PCL films;[54]
- *in vitro* paclitaxel release from poly(lactide-*co*-caprolactone) (PLACL) coated stent;[55]
- *in vitro* rapamycin release from PLGA coated DES and film mass loss during degradation times;[52]
- *in vitro* heparin release from poly-L-lactide acid (PLLA) film;[56]
- *in vitro* bovine aortic SMC (BASMC) growth inhibition in different paclitaxel solution;[57]
- *in vitro* proliferation assays of vascular SMC (VSMC) obtained from human saphenous veins;[58]
- *in vivo* neointimal thickening inhibition (in a pig model) via paclitaxel intravenous administration;[57]
- *in vivo* neointimal thickening inhibition (in a rabbit model) via paclitaxel release from PLACL coated DES;[55]
- *in vivo* neointimal thickening inhibition (in a pig model) via paclitaxel release from PLGA coated DES.[53]

Accordingly, our aim here was to develop a mathematical model to investigate the influence of coating design parameters and drug properties on release kinetics, taking also into account SMC proliferation. That model should be simple with respect to numerical solution (thus avoiding computational expensive simulations, as happens with FEM), but at the same time it should be able to take into account all fundamental phenomena that influence the final behavior.

2. MODEL DEVELOPMENT

It is generally accepted that drug release from a resorbable matrix depends on both polymer degradation and drug molecular diffusional transport.[59] Indeed, drug release phenomena are generally known to follow Fick's laws and to take place in three steps: a slow diffusion is followed by a fast one that precedes general device degradation. As polymer degradation increases, diffusional paths open through the polymer matrix pores, allowing solvated drug molecules to leave the device via degradation-controlled release.[59] This behavior is also particularly relevant when drug loading is generally lower than 5% (w/w),[59] a condition generally satisfied in both experimental systems and commercial devices. As mentioned, the aim of this work was the development of a mathematical model able to take into account all involved phenomena: polymer degradation, drug release, and neointimal thickening. In this way, indeed, it is possible to evaluate stent performances with respect to a certain number of design parameters such as material formulation (which determines degradation kinetics), drug loading conditions, and coating thickness. The effect of the growth of neointimal tissue embedding the device was also considered, to properly characterize stent behavior in *in vivo* conditions. A schematic representation of the phenomena involved after the implantation of a biodegradable polymer-based DES and of drug delivery mechanisms is visible in Figure 1.

2.1. Polymer Degradation. The degradation model is based on the formalism proposed by Arosio et al.[60,61] for aliphatic polyesters, since available experimental data regard this

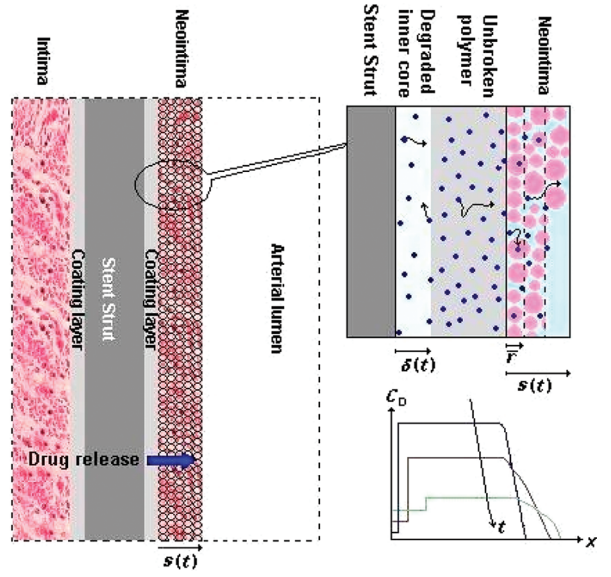

Figure 1. Schematic representation of the phenomena involved after the implantation of a biodegradable polymer-based DES and drug delivery mechanisms (C_D, drug concentration).

very common kind of biopolymers. Aliphatic polyester degradation is due to the hydrolysis mechanism, which can show two macroscopic behaviors depending on the thickness of the device, where a critical thickness can be defined according to polymer characteristics.[62] In the case of thick devices, water penetrates into the device and cleaves the polymer backbone, producing small oligomers. These chain fragments are not able to diffuse properly from the matrix, and, moreover, they catalyze a hydrolysis reaction because of their acidic groups.[63] In this case, also known as bulk degradation, occurring phenomena allow adopting a shrinking core approach, in which the system can be roughly divided in two zones: a degraded inner core and an external shell of unbroken polymer.[61] On the other hand, degradation dynamics could be described in detail through mass conservation equations, where diffusion phenomena are neglected because of the low polymeric thickness, which is less than critical value (usually in the range of the hundreds of micrometers); this is the case of the so-called surface degradation.[62]

The enzyme role in polymer degradation in the *in vivo* environment has been found to depend on polymer hydrophilicity and molecular weight.[64−67] In particular, enzymatic degradation becomes less important with the increase of polymer molecular weight and the decrease of water uptake. Indeed, adding lactide and/or lactone units, which are more hydrophobic than glycolic ones, causes a lower water uptake and thus a less important enzymatic contribution on the device degradation.[68] As far as devices investigated were made of PCL, PLACL, and PLGA with a high content of lactide units, and with a molecular weight of about 10^3 kDa, enzymatic contribution in polymer hydrolysis was reasonably neglected. As regards the pH effect, during the degradation of aliphatic polyesters, such as PLLA, PGA, and PCL, the most relevant contribution in pH decreasing is due to acidic oligomers deriving from device hydrolysis. Indeed, as reported by Holy et al.,[69] macrophages are called-in and activated by the local inflammation, and they contribute to a pH reduction down to a value of about 5, while the influence of pH of surrounding medium becomes important with very acidic pH.[67]

Mass fluxes are expressed with an effective mass transport coefficient and a concentration difference between the polymeric phase and the external environment. Moreover, it was assumed that only monomers could leave the matrix because of the low mobility of chain fragments. The adopted kinetic scheme is a reversible polycondensation: $P_{n+m} + W \leftrightarrow P_n + P_m$. Polymer degradation can thus be described through three mass balances involving monomer, water, and *n*-long polymer chains, respectively:

$$\frac{dC_M}{dt} = k_{C,M}\frac{S_{EXT}}{V_M}(C_M^0 - C_M) - 2k_P C_M \sum_{n=1}^{\infty} C_n + 2\frac{k_P}{K_{EQ}} C_W \sum_{n=2}^{\infty} C_n \quad (1)$$

$$\frac{dC_W}{dt} = k_{C,W}\frac{S_{EXT}}{V_R}(C_W^0 - C_W) + k_P \sum_{n=1}^{\infty} C_n \sum_{m=1}^{\infty} C_m - \frac{k_P}{K_{EQ}} C_W \sum_{n=1}^{\infty} (n-1)C_n \quad (2)$$

$$\frac{dC_n}{dt} = k_P \sum_{j=1}^{n-1} C_j C_{n-j} - 2k_P C_n \sum_{j=1}^{\infty} C_j + 2\frac{k_P}{K_{EQ}} C_W \sum_{j=n+1}^{\infty} C_j - \frac{k_P}{K_{EQ}} C_W (n-1) C_n \quad (3)$$

where C_i, C_i^0, and $k_{C,i}$ are the molar concentration, the molar concentration in the external environment, and the effective mass transport coefficient for the *i*-th species, respectively; k_P is the polymerization kinetic constant, K_{EQ} is the polymerization equilibrium constant, S_{EXT} is the external coating surface, V_R is the device volume, and V_M is the volume of the degraded inner zone. To simplify the model, which would result in a large system of differential equations, the method of moments was here applied. Since water and monomer mass balance equations (eqs 1 and 2) can be written in terms of statistical moments (μ_i), the following system is obtained:

$$\frac{dC_M}{dt} = k_{C,M}\frac{S_{EXT}}{V_M}(C_M^0 - C_M) - 2k_P C_M \mu_0 + \frac{k_P}{K_{EQ}} C_W(\mu_0 - C_M) \quad (4a)$$

$$\frac{dC_W}{dt} = k_{C,W}\frac{S_{EXT}}{V_R}(C_W^0 - C_W) + k_P \mu_0^2 - \frac{k_P}{K_{EQ}} C_W(\mu_1 - \mu_0) \quad (4b)$$

$$\frac{d\mu_0}{dt} = k_{C,M}\frac{S_{EXT}}{V_M}(C_M^0 - C_M) - k_P \mu_0^2 + \frac{k_P}{K_{EQ}} C_W(\mu_1 - \mu_0) \quad (4c)$$

$$\frac{d\mu_1}{dt} = k_{C,M}\frac{S_{EXT}}{V_M}(C_M^0 - C_M) \quad (4d)$$

$$\frac{d\mu_2}{dt} = k_{C,M}\frac{S_{EXT}}{V_M}(C_M^0 - C_M) + 2k_P \mu_1^2 + \frac{k_P C_W}{3K_{EQ}}\left(\mu_1 - 2\frac{\mu_2^2}{\mu_1} + \frac{\mu_2 \mu_1}{\mu_0}\right) \quad (4e)$$

Quantities such as average molecular weight and polydispersity can be directly computed from statistical moments. This approach was explained in detail and validated in our earlier works.[60,61]

2.2. Neointimal Thickening: Corpuscular Approach. To describe the proliferation of SMC, both in *in vitro* and *in vivo* conditions, the corpuscular approach proposed by Busini et al.[70] was here adopted. The time evolution of cells number can be expressed through a population balance equation as follows:

$$\frac{\partial F(m,t)}{\partial t} + \frac{\partial}{\partial m}(F(m,t)g(\mathbf{X})) = M(m,\mathbf{X})F(m,t) - d(\mathbf{X})F(m,t) \quad (5)$$

where $F(m,t)$ is the cell number whose mass is comprised between m and $m + dm$ at time t, $g(\mathbf{X})$ represents cell growth, $d(\mathbf{X})$ represents cell death because of apoptosis and necrosis, $M(m,\mathbf{X})$ represents cell replication by mitosis, and $\mathbf{X}$ is the parameter vector, containing quantities such as substrate and drug concentrations. Equation 5 was solved introducing the expressions of three moments λ_i, that represents the *i*-th order

statistical moment of the distribution function $F(m)$, in particular: λ_0 represents the overall number of cells, and λ_1 represents the mass of the tissue. Indeed, in the second equation the term describing cell mitosis does not appear, since it does not influence the mass of the tissue. Finally, it is necessary to choose a probability function for cellular division to solve the problem. A simple step function is here adopted, meaning that cells divide only when they reach the critical mass value m^*. The final system is thus the following:

$$\frac{\partial\lambda_0}{\partial t} = -d(\mathbf{X})\lambda_0 + g(\mathbf{X})F(m^*) \tag{6a}$$

$$\frac{\partial\lambda_1}{\partial t} = g(\mathbf{X})\lambda_0 - d(\mathbf{X})\lambda_1 \tag{6b}$$

$$\frac{\partial\lambda_2}{\partial t} = 2g(X)\lambda_1 - d(\mathbf{X})\lambda_2 - \frac{1}{2}g(\mathbf{X})(m^*)^2F(m^*) \tag{6c}$$

However, this formulation requires the value of $F(m^*)$; because of the lack of information about the real form of the distribution function, an unimodal log-normal distribution function for cell masses is chosen:[70]

$$F(m) = \frac{\lambda_0}{3\sqrt{2\pi}\ln\sigma}\frac{1}{m}\exp\left[-\frac{\ln^2(m/m_g)}{18\ln^2\sigma}\right] \tag{7}$$

Following the approach of Busini and co-workers,[70] it is possible to evaluate the instantaneous thickness of cell growing multilayer $s(t)$, being described as follows:

$$s(t) = r^{ave}\frac{\lambda_0}{N_{max}} \tag{8}$$

where λ_0 is the zero-order moment, N_{max} is the maximum number of cells allowed in each proliferating layer, defined as the ratio between the cross section area occupied by a single layer A_{cross} and the coating surface area S_{Ext}:

$$N_{max} = \frac{A_{cross}}{S_{Ext}} \tag{9}$$

$$A_{cross} = \pi\left(\frac{3V_L}{4\pi}\right)^{2/3} \tag{10}$$

V_L is the total volume of cell population:

$$V_L = \frac{\lambda_1}{\rho_{cell}} \tag{11}$$

The term λ_0/N_{max} in eq 8 represents the number of single layers constituting the cell front; r^{ave} is the average radius of a single layer, computed as follows:

$$r^{ave} = \left(\frac{3V_L}{4\pi\lambda_0}\right)^{1/3} \tag{12}$$

2.3. Drug Release. Drug release is described both for *in vitro* and *in vivo* conditions by means of specific equations that are different with respect to the considered environment. In general, the drug is solubilized in the inner core up to its solubilization limit, and it then diffuses toward the surrounding environment. For what concerns *in vitro* release in aqueous solution, the approach proposed by Arosio et al.[60] is here adopted. The model assumes that the initial drug amount is divided in equal particles with a certain diameter d_p, uniformly distributed into the device. Solubilization dynamics can be thus described as follows:

$$\rho_D\frac{d}{dt}\left(\frac{n_p^0\pi d_p{}^3}{6}\right) = -k_{C,sol}(C_{Int}^{sat} - C_{Int})\pi d_p{}^2 \tag{13}$$

where ρ_D is drug density, n_p^0 is the initial number of drug particles, k_C is the solubilization mass transfer coefficient, C_{Int}^{sat} is the drug solubility in water, and C_{Int} is the concentration of solubilized drug into the inner core of the device. Another equation is then needed to characterize the time evolution of the solubilized drug:

$$\varepsilon_{poly}\frac{d}{dt}\left(\frac{C_{int}V_MC_W}{\rho_W}\right) = n_p^0k_{C,sol}(C_{Int}^{sat} - C_{Int})\pi d_p{}^2 - k_{C,ext}S_{ext}(C_{Int} - C_{ext}) \tag{14}$$

where ε_{poly} is polymer void fraction, $k_{C,ext}$ is the effective mass transfer coefficient, S_{ext} is the interface between water solution and nondegraded polymer, and C_{ext} is drug concentration in the external solution. Finally, a third equation completes the model describing the dynamics of drug release in external solution:

$$V_{ext}\frac{dC_{ext}}{dt} = k_{C,ext}S_{ext}(C_{Int} - C_{ext}) \tag{15}$$

where V_{ext} is the volume of the external solution. To describe drug distribution into neointimal tissue, the growing tissue is assumed to be composed by two phases: cellular and extracellular. The former is composed by SMC only, while the latter comprehends water and both cellular debris and byproducts. The overall dissolution rate, referring to the extracellular phase, can be expressed as follows:

$$\Delta_D = N\rho_Dk_{C,sol}(C_{ext}^* - C_{ext})\pi\left(\frac{6n_D}{\pi\rho_D}\right)^{2/3} \tag{16}$$

where N is the number of drug particles per unit coating volume, n_D is the number of drug moles in a solid particle, C_{ext} is the drug concentration in the extracellular phase, and C_{ext}^* is the saturation value. The adsorption kinetics can be described through mass balances referring to cellular and extracellular phases, respectively:

$$\varepsilon_{tiss}\frac{dC_{ext}}{dt} = -\frac{k_{C,ext}S_{ext}}{V_{ext}}(C_{coat} - C^*{}_{ext}) + \Delta_D \tag{17a}$$

$$(1 - \varepsilon_{tiss})\frac{dC_L}{dt} = -\frac{k_US_L}{V_L}(C_L^* - C_L) - R_L \tag{17b}$$

where ε_{tiss} is the tissue porosity, V_{ext} and S_{ext} are the volume and the surface area of the extracellular phase, respectively, $k_{C,ext}$ is the mass transfer coefficient for the extracellular phase side, C_{coat} is the drug concentration within polymer coating, k_U is the overall drug uptake coefficient, V_L and S_L are the volume and the surface area of the cellular phase, respectively, and C_L^* is the saturation value in the cellular phase. Equilibrium concentrations into cellular and extracellular phase are correlated by means of a binding capacity coefficient:

$$C^*{}_L = K_DC_{ext}^* \tag{18}$$

dx.doi.org/10.1021/mp200573f | *Mol. Pharmaceutics* 2012, 9, 1898–1910

Table 1a. *In Vitro* Polymer Degradation for Different Polymer Films

	unit	Lu et al.[50]		Lao et al.[51]	
				pactitaxel	
polymer composition		PLGA	PLGA	PLGA	PLGA
		50:50	75:25	53:47	53:47
film thickness	cm	1.00×10^{-3}	9.00×10^{-3}	3.00×10^{-3}	8.00×10^{-3}
film surface area	cm^2	1.13	1.13	1	1
polymer molecular weight	g/mol	3.73×10^4	3.43×10^4	9.00×10^4	9.00×10^4
monomer molecular weight[a]	g/mol	83	83	83	83
polymer density	g/cm^3	1.19	1.31	1.2	1.2
initial monomer concentration	mol/cm^3	1.00×10^{-6}	1.00×10^{-6}	1.00×10^{-6}	1.00×10^{-6}
initial water concentration	mol/cm^3	0	0	0	0
water diffusivity	cm^2/s	1.00×10^{-6}	1.00×10^{-6}	1.00×10^{-6}	1.00×10^{-6}
water equilibrium concentration	g/cm^3	1	1	1	1
monomer diffusivity	cm^2/s	1.00×10^{-10}	1.00×10^{-10}	1.00×10^{-10}	1.00×10^{-10}
kinetic constant[b]	$cm^3/s/mol$	1.00×10^{-9}	1.00×10^{-9}	2.00×10^{-9}	5.00×10^{-9}
equilibrium constant		1.00×10^{-3}	1.00×10^{-3}	1.00×10^{-3}	1.00×10^{-3}
pd		8.9	8.9	n.a.	n.a.
degradation time	weeks	<4	<4	<4	<3
integration step	h	1.00×10^{-3}	1.00×10^{-3}	1.00×10^{-3}	1.00×10^{-3}

[a]Calculated as the arithmetic mean between PLA and PGA molecular weights. [b]Fitted from experimental data.

Table 1b. *In Vitro* Drug Release and Polymer Degradation for Different Polymer Films and Stents

	unit	Jabara et al.[53]	Lao et al.[51]	Pan et al.[52]	Drachman et al.[55]	Tan et al.[56]
		paclitaxel	paclitaxel	rapamycin	paclitaxel	heparin
polymer composition		PLGA	PCL	PLGA	PLACL	PLLA
		stent		stent	stent	film
film or coating thickness	cm	8.00×10^{-4}	7.50×10^{-3}	1.00×10^{-3}	2.00×10^{-3}	1.00×10^{-2}
film or coating surface area	cm^2	2.52[b]	1.44	1.24[b]	1.35[b]	1.4
polymer molecular weight	g/mol	100000	8.00×10^4	9.58×10^4	140000	3.30×10^6
monomer molecular weight	g/mol	83[a]	114	83[a]	114	90
polymer density	g/cm^3	1.2[b]	1.1[b]	1.2[b]	1.4[b]	1.3[b]
initial monomer concentration	mol/cm^1	1.00×10^{-10}	1.00×10^{-10}	1.00×10^{-10}	1.00×10^{-10}	1.00×10^{-10}
initial water concentration	mol/cm^3	0	0	0	0	0
water diffusivity	cm^3/s	1.00×10^{-6}	1.00×10^{-6}	1.00×10^{-6}	1.00×10^{-6}	1.00×10^{-6}
water equilibrium concentratio	g/cm^3	1	1	1	1	1
monomer diffusivity	cm^2/s	1.00×10^{-10}	1.00×10^{-10}	1.00×10^{-10}	1.00×10^{-10}	1.00×10^{-10}
kinetic constant[b]	$cm^3/s/mol$	5.00×10^{-9}	1.00×10^{-8}	5.00×10^{-9}	1.00×10^{-11}	1.00×10^{-12}
equilibrium constant		1.00×10^{-3}	1.00×10^{-3}	1.00×10^{-3}	1.00×10^{-3}	1.00×10^{-3}
degradation time	weeks	n.a.	>20	<4	>25	>30
drug molecular weight	g/mol	854	854	914	854	13500
drug diffusivity[b]	cm^2/s	1.00×10^{-9}	1.00×10^{-8}	1.00×10^{-8}	1.00×10^{-11}	1.00×10^{-12}
drug percent (w/w)		10%	10%	15%-40%	25%	10%
integration step	h	1.00×10^{-3}	1.00×10^{-3}	1.00×10^{-3}	1.00×10^{-3}	1.00×10^{-3}

[a]Calculated as the arithmetic mean between PLA and PGA molecular weights. [b]Fitted from experimental data.

Furthermore, R_L is the drug elimination rate due to pharmacokinetics, and it is expressed through a first-order kinetic law:

$$R_L = k_{el} C_L \tag{19}$$

where k_{el} is the first-order elimination constant.

2.4. Model Parameter Estimation. Besides parameters defining device geometry, model parameters relate to polymer degradation kinetics (i.e., k_p and K_{EQ}), species effective diffusivities within each phase (i.e., D_M, D_W, D_D) and phase porosities (i.e., ε_{poly}, ε_{tiss}). Moreover, drug solubility limits in water, its binding properties (i.e., K_D and k_U), and kinetic parameters describing neointimal thickening inhibition are also needed. Spatial independence for all physical-chemical and transport properties was assumed. The degradation kinetics parameters are, as said, polymer-dependent: in particular, the attention was focused on the most commonly used polyesters: PLGA, having different copolymer ratios (75:25,[50] 50:50,[50] 53:47[51,52]), PCL,[54] PLACL,[55] and P$_L$LA[56] films.

All adopted values are summarized in Tables 1a and 1b.

Relative to drug transport mechanisms through artery wall tissue, many available models are based on theories on solute transport through porous media:[71] Briefly, the key phenomenon is represented by the collisions of large molecules with the structure of the extracellular matrix resulting in a reduced diffusional transport due to the decrease in molecular mean free path. Nevertheless, once again, their reliability has yet to be confirmed for drugs having different solubilization dynamics, different molecular hydrodynamics, and different binding mechanisms.

Results achievable nowadays are provided by the "free-volume" theory,[72] even if it presents a relatively large number of input parameters seldom estimable from pure component data. Hence, for each phase (i.e., polymer and tissue) a hindrance coefficient, ε_v, and a tortuosity factor, τ_v, (v = polymer, tissue) were introduced to estimate the effective diffusivity from the knowledge of the asymptotic value for the drug diffusion coefficient in the liquid phase $D_{j,L}$ (j = M, W, D):

$$D_j = D_{j,L} \cdot \frac{\varepsilon_v}{\tau_v} \tag{20}$$

The adopted idealized tissue morphology (see Figure 1) also allows estimating tissue porosity from the knowledge of the extracellular volume fraction (p).

Drug solubility is a standard thermodynamic parameter, and it is usually known for any of the commercial drug compounds. Nevertheless, for example, literature suggests that there is more than one solid-state form of paclitaxel having different aqueous solubility limits. Although, in literature, such a behavior has not been explained in detail yet, estimates are in the range of 0.7–30 μg/cm^3[51,73] depending on the amount of organic compounds added to enhance drug aqueous solubility. Analogous considerations are valid for rapamycin, whose solubility in water is 2.6 μg/cm^3, but strongly depend on the addition of pure cosolvents.[52,74]

Moreover, drug tissue binding parameters (i.e., k_U, K_D) for paclitaxel and rapamycin were estimated by fitting eqs 17a and 17b onto data obtained by selected reaction monitoring liquid chromatography tandem mass spectrometry analysis and recently also by tissue loading–elution and transmural diffusivity experiments.[29,75]

Furthermore, the richness in data of the two proliferation assays[57,58] allowed the estimation of some parameters governing the growth process in the first stage of the SMC proliferation in unperturbed growth regime (drug-free conditions). In particular, the values of the child mass and the division mass were calculated starting from the maximum number of cells and imposing a cell density of 1.1 g/cm^3.[70] All of these parameters are reported in Table 2.

Table 2. Summary of Physiological Data Used for the *in Vitro* SMC Growth Simulations

	unit	Scheller et al.[57]	Marra et al.[58]
cell line		BASMC	VSMC
mass of the child SMC	g	4.32×10^{-9}	4.32×10^{-9}
division mass of the mother SMC	g	8.64×10^{-9}	8.64×10^{-9}
yield growth coefficient		0.4	0.4
glucose external concentration	g/L	1.2[a]	1.0
glucose critical concentration	g/L	1.00×10^{-2}	1.00×10^{-2}
beginning proliferating medial SMC mass	g	5.00×10^{-5}	5.80×10^{-5}

[a]Fitted from experimental data.

Because of the lack of reliable quantitative studies and well-established theories on SMC apoptosis, all other kinetic parameters introduced in the corpuscular approach and the glucose and oxygen diffusivities were determined to best-fit the experimental data for each cell line examined.[57,58] All obtained values are summarized in Table 3.

2.5. Numerical Solution. The overall model is constituted by the systems of described differential equations and do not admit analytical solutions because of the complexity of the set of population equations. Only numerical solutions are thus feasible for practical purposes: the systems were integrated through the fourth-order Runge–Kutta method with time discretization reported in Tables 1 and 3.

Table 3. Specific Growth Parameters (Fitted Experimental Data)

	unit	Scheller et al.[57]	Marra et al.[58]
cell line		BASMC	VSMC
glucose diffusivity	cm^2/s	1.20×10^{-6}	1.20×10^{-6}
specific glucose uptake	g/cell/h	5.70×10^{-12}	5.00×10^{-11}
maximum growth rate	1/h	1.69×10^{-2}	1.71×10^{-2}
half-rate constant	g/cell/L	8.55×10^{-8}	1.20×10^{-7}
necrosis death rate	1/h	2.70×10^{-7}	3.25×10^{-7}
minimum apoptosis rate	1/h	7.50×10^{-7}	8.00×10^{-7}
maximum apoptosis rate	1/h	4.30×10^{-5}	6.20×10^{-5}
efficacy constant	L/mg/h	120	34
elimination rate constant	1/h	5.70×10^{-2}	1.70×10^{-2}
integration step	h	1.0×10^{-3}	1.0×10^{-3}

3. MODEL VALIDATION AND DISCUSSION

3.1. *In Vitro* Drug Release and Polymer Degradation. In the first two examined cases, authors investigated the *in vitro* hydrolytic degradation of PLGA films.[50,51] In particular, they focused their attention on the effect of film thickness and copolymer ratio on degradation dynamics. Results showed that thick films degrade faster than thin ones, in agreement with the general degradation mechanism accepted in literature and explained above: indeed, in thick films acidic oligomers diffuse slower out the matrix increasing their catalytic effect on hydrolysis reaction by locally lowering the inner matrix pH.[64] Moreover, the increase of glycolic groups percentage in polymer composition seems to accelerate the degradation rate for films having the same thickness. This is due to the higher hydrophilicity of glycolic groups with respect to the lactic ones. The model quantitatively well matches the observed experimental trends (Figures 2 and 3).

Pan et al.[52] monitored the mass loss and water absorbance for thin PLGA film (i.e., 10 μm): again model predictions are in good agreement with experimental data (Figure 4).

After having positively assessed model reliability in predicting polymer degradation, a wide set of experimental data available from several different systems was used to validate model capacity to describe both the drug release behavior and the influences of initial drug loading and polymer formulation on drug release kinetics. In the third case examined,[53] the authors monitored the *in vitro* paclitaxel release from thin PLGA coated DES and hydrolytic degradation of the stent coating. These lightly loaded devices present a mild initial burst release, probably due to the immediate dissolution of drug on the external coating surface. This is followed by a period of moderate release, which is believed to correspond to drug diffusion out of the hydrated but intact polymer. The diffusion release phase then flattens out, followed by a release rate subsequent increase after 50 days, in correspondence with an increase in the erosion rate of the polymer, which finally tapers off again as 90% or more of the drug is released (Figure 5).

In another work, Lao et al.[54] studied the paclitaxel release from PCL film: PCL formulation, due to its slow degradation rate, did not permit avoiding the "burst effect", which was also followed by a diffusion-governed stage (Figure 6, red line and

dx.doi.org/10.1021/mp200573f | Mol. Pharmaceutics 2012, 9, 1898–1910

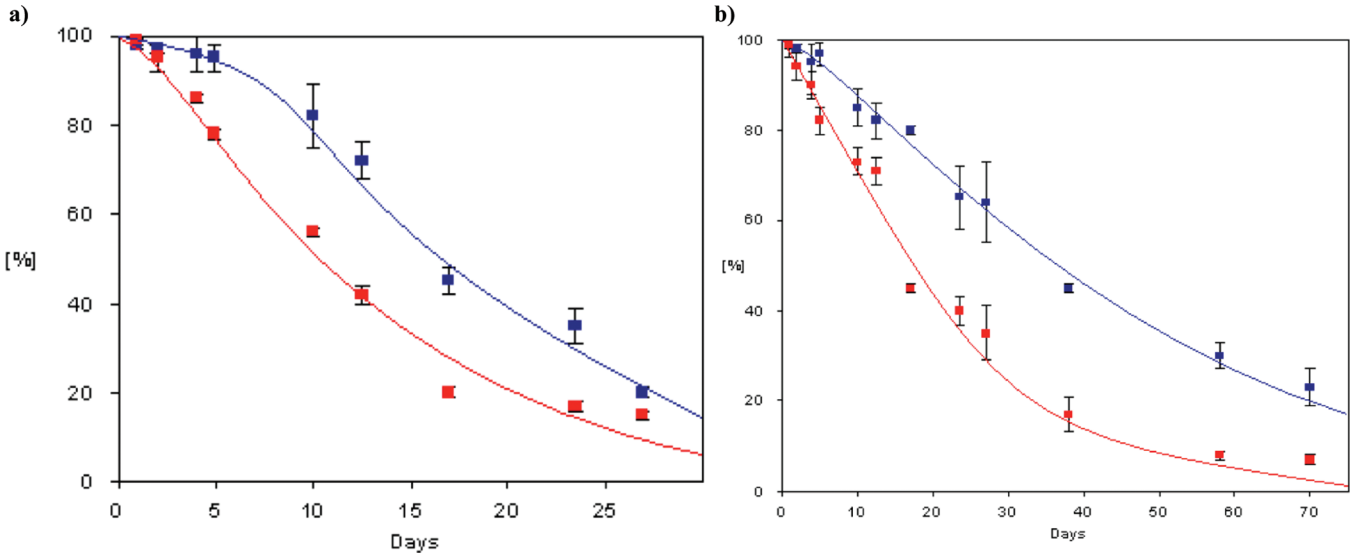

Figure 2. Comparison between experimental and calculated average molecular weight decay for (a) PLGA 50:50 films having different thicknesses (10 and 90 μm with s.d. = 12.4 and s.d. = 14.3, blue and red lines, respectively); (b) PLGA 75:25 films having different thicknesses (10 and 90 μm with s.d. = 3.5 and s.d. = 5.8, blue and red lines, respectively). Experimental data are taken from ref 50.

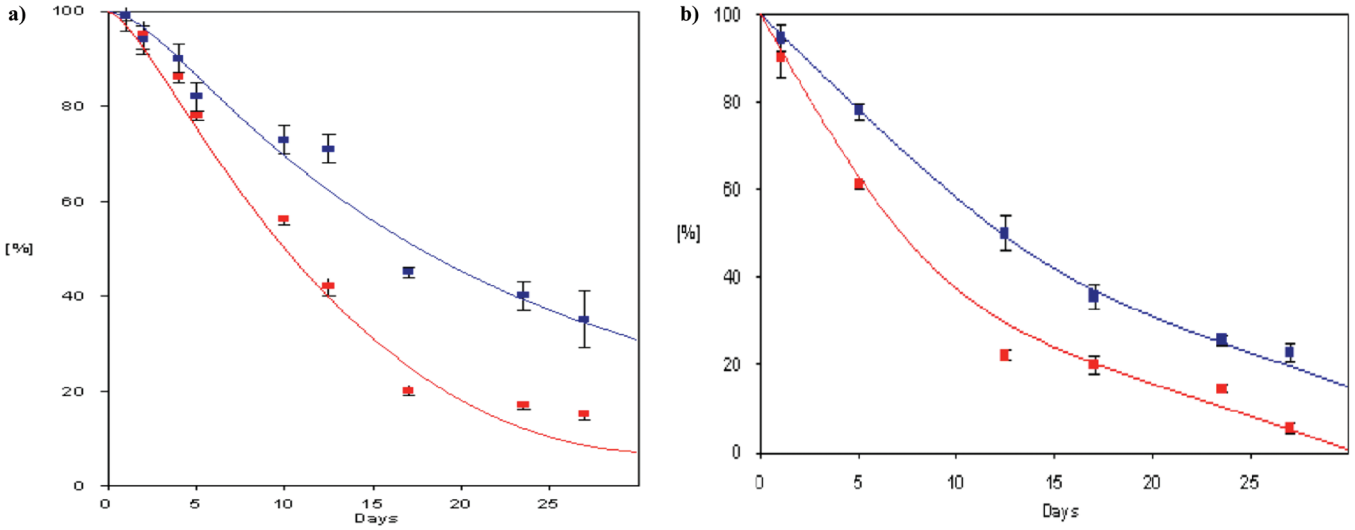

Figure 3. Comparison between experimental and calculated average molecular weight decay for (a) thick (80 μm) PLGA films having different copolymer ratios (50:50 and 75:25 with s.d. = 7.5 and s.d. = 4.7, red and blue lines, respectively); (b) PLGA 53:47 films having different thicknesses (30 and 80 μm with s.d. = 1.5 and s.d. = 4.5, blue and red lines, respectively). Experimental data are taken from ref 51.

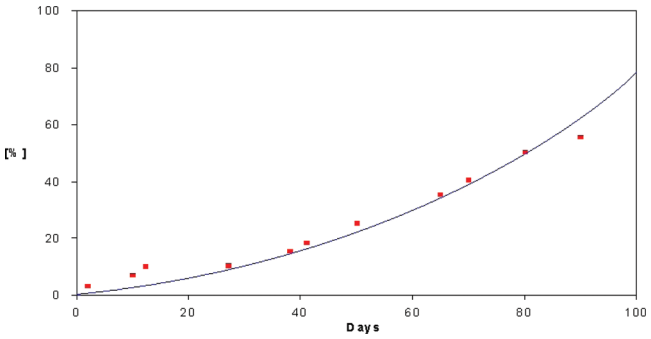

Figure 4. Comparison between experimental and calculated film mass loss during degradation for thin (10 μm) PLGA film (s.d. = 4.3). Experimental data are taken from ref 52.

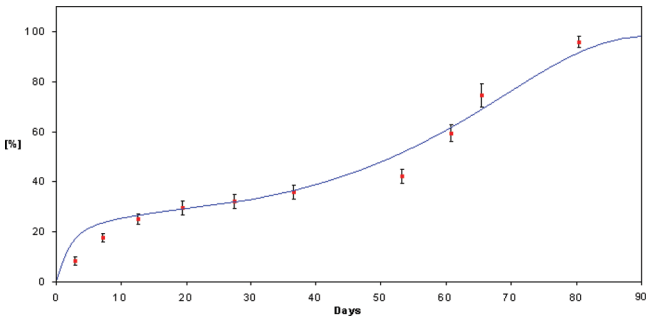

Figure 5. Comparison between experimental and calculated paclitaxel cumulated release from thin PLGA coated DES (s.d. = 7.3). Experimental data are taken from ref 53.

dots). Drachman et al.[55] characterized the behavior of DES's coated with PLACL (Figure 6, blue line and dots): devices were

dx.doi.org/10.1021/mp200573f | *Mol. Pharmaceutics* 2012, 9, 1898–1910

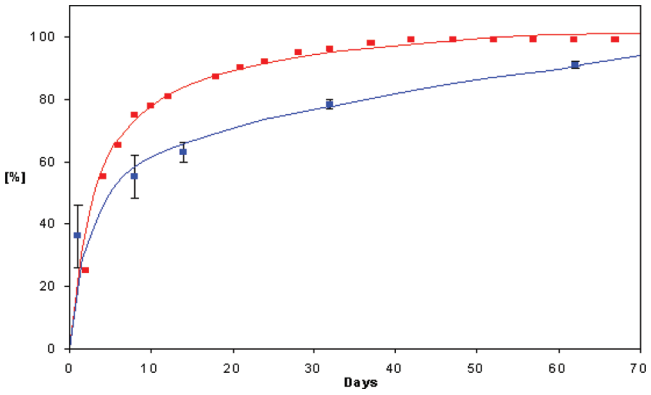

Figure 6. Comparison between experimental and calculated paclitaxel cumulated release from thick PLC and PLACL films (s.d. = 2.1 and s.d. = 2.8, red and blue lines, respectively). Experimental data are taken from refs 54 and 55, respectively.

immersed in 15 mL of calf serum, and then they were removed regularly at 1,7, 14, 28, and 56 days from their release vials and analyzed for residual paclitaxel content by high-performance liquid chromatography (HPLC). Serum was refreshed every day to ensure sink conditions. Once again, our model simulations also match this set of experimental data well.

Furthermore, Pan et al.[52] also monitored rapamycin release from PLGA coated DES's, and in particular, their attention was focused on the influence of the amount of loaded drug (drug-to-polymer ratios: 15% and 40%, w/w) on the release profile which, too, are very well matched by our model previsions (Figure 7).

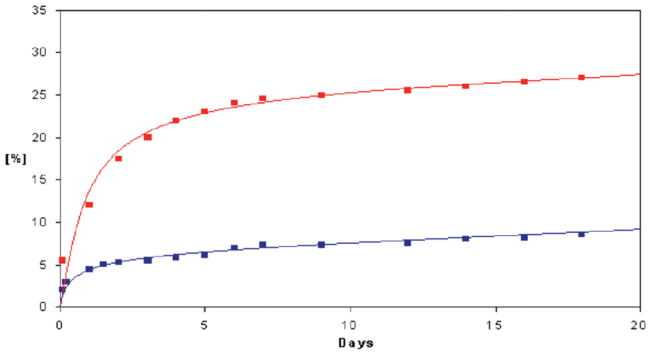

Figure 7. Comparison between experimental and calculated rapamycin cumulated release from thin (10 μm) PLGA 53:47 film for low and high drug loadings (15 wt % and 40 wt % with s.d. = 1.1 and s.d. = 1.4, blue and red lines, respectively). Experimental data are taken from ref 52.

All of the examined cases confirm that the overall degradation kinetics is in agreement with that of an autocatalytic process,[61,76] with a consequent exponential production of oligomers within the polymer structure and, thus, a decrease of the polymer molecular weight. Moreover, mass loss (due to the diffusional release of monomer) exhibits a linear trend throughout the degradation process, after the inactive period when the water absorption occurs.

The aqueous solubility and the lipophilic nature of the examined drugs strongly influence the drug release kinetics. In particular, Tan et al.[56] showed that the low solubility of the hydrophilic drug (e.g., heparin) in hydrophobic polymer matrices could enhance the burst effect, as a large fraction of the drug diffuse outside the polymer matrix in the very first time frame: solubilization dynamics can indeed be neglected, being much faster than release ones. This evidence is well-described also by simulations (Figure 8).

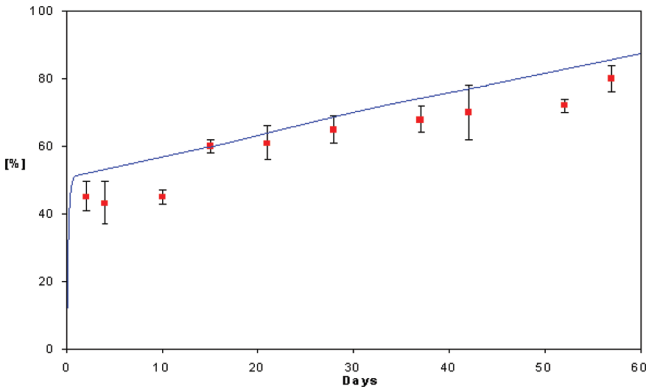

Figure 8. Comparison between experimental and calculated heparin cumulated release from thick (100 μm) PLLA film (s.d. = 6.5). Experimental data are taken from ref 56.

On the contrary, in the case of highly hydrophobic drugs (e.g., paclitaxel and rapamycin), the drug solubilization dynamics in water phase cannot be neglected because of the strong contribution on drug release rate decrease[61] (Figures 4 and 7). Moreover, even if an initial (undesired) drug dissolution is always present due to the Brownian molecular motion of the drug particles through the polymer matrix, its contribution to the instantaneous amount of drug released can be diminished by adjusting the drug-to-polymer ratios toward values less than 5% (w/w) (Figure 7). With the increase of drug-to-polymer ratio, the release rate increases; however, the drug release profile is not proportionally linear with the drug loading increase, as evident also from data and plots reported in Figure 7.

The model here developed quantitatively matches the experimental trend on the drug release well, as well as on the degradation behavior depending on coating thickness and polymer formulation for *in vitro* conditions. In particular, in order to ensure a sustained release rate, our results suggest to adopt lightly loaded (<5% w/w) thin (<10 μm) films, having a copolymer ratio in favor to PLA. Indeed, a low coating thickness[62,63] and the hydrophobic behavior, due to PLA lactide units, promote the surface erosion mechanism, improving release rate control. Our simulations allowed us to define an optimal interval values for the design parameters to achieve a tailored release and, hence, to avoid possible risk of toxicity (i.e., local drug concentrations in the living phase surrounding the coating higher than the threshold toxic value[77]).

3.2. *In Vitro* SMC Growth and Neointimal Thickening.

The influence, on drug release kinetics, of living tissues surrounding the device was reported with *in vitro* proliferation assays that considered different cell lines (BASMC,[57] VSMC[58]) in the presence of different cell growth inhibitors (paclitaxel,[57] salicylate[58]). In the first case,[57] BASMC were cultured using Dulbecco's modified Eagle's medium (DMEM) supplemented with 10% fetal bovine serum (FBS). Cells were seeded at 1×10^4 cell/cm^2 and incubated for 3, 10, or 60 min with 0.9% saline (control) and iopromide supplemented with paclitaxel. The supernatant was then removed, and cells were washed with 0.9% saline and cultured with DMEM plus 10% FBS. At days 0,

dx.doi.org/10.1021/mp200573f | *Mol. Pharmaceutics* 2012, 9, 1898–1910

3, 6, 9, and 12, cell counts were performed. The *in vitro* experiments indicated that short contact times with iopromide paclitaxel induce an almost complete inhibition of vascular smooth muscle cell proliferation. The growth model simulation is presented in Figure 9 and matches the experimental trends well.

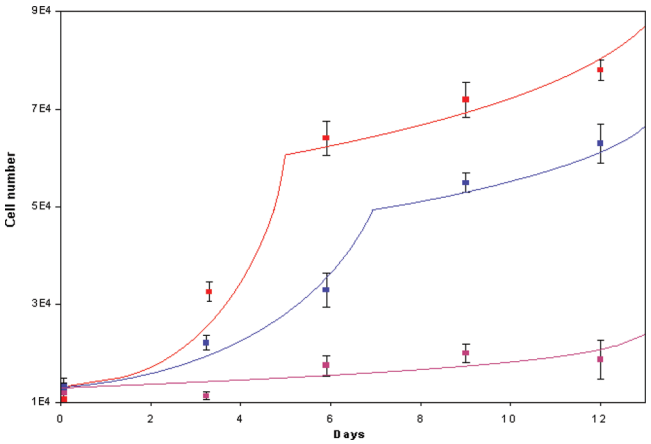

Figure 9. Comparison between experimental and calculated BASMC growth in the presence of different paclitaxel concentration (drug-free, 1.46 μM and 14.6 μM, with s.d. = 2.8 × 10^3, s.d. = 2.9 × 10^3, s.d. = 2.7 × 10^3, red, blue, and violet lines, respectively). Experimental data are taken from ref 57.

Moreover, Marra et al.[58] studied the salicylate inhibitory action on vascular SMC growth. The comparison between experimental data and our model is presented in Figure 10.

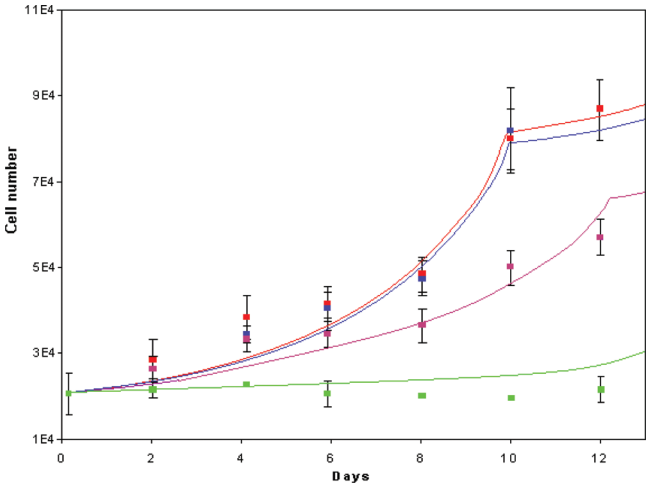

Figure 10. Comparison between experimental and calculated hVSMC growth in the presence of different salicylate concentrations (drug-free, 0.1 mM, 1 mM, and 5 mM, with s.d. = 6 × 10^3, s.d. = 5.6 × 10^3, s.d. = 6 × 10^3, and s.d. = 5 × 10^3, red, blue, violet, and green lines, respectively). Experimental data are taken from ref 58.

Cells, incubated in growth medium alone, grew exponentially through day 10, reaching a plateau at day 12. In a concentration-dependent manner, the drug addition inhibited SMC proliferation. Low salicylate local concentrations (<0.1 mM) did not affect the cell number compared with controls, while 1 mM salicylate led to a reduction in SMC growth beginning at day 4 and resulting in an efficient (about 33%) growth inhibitory action at day 10. The same authors also assessed the reversibility of this growth-inhibitory effect, by replacing the medium with a drug-free one. The removal of salicylate from the medium led SMC to a re-entrance into the growth phase at a rate comparable to that of controls. The results of all of these studies, for unperturbed cellular proliferation, showed the typical "hill and valley" growth pattern where an exponential rapid growth is followed by a smooth one, mainly due to the onset of apoptosis.[78] The change in the curvature of model obtained plots reported in Figures 9 and 10 highlights the influence of apoptosis in the cellular growth process (in drug-free conditions) well.

As mentioned above, interactions between drug and mechanisms governing apoptosis are more complex. In particular, paclitaxel inhibited cell proliferation in a dose-dependent manner. Coronary artery endothelial cells are highly sensitive to the antiproliferative effects of paclitaxel, exhibiting near-complete inhibition of proliferation with just two days of continuous exposure, and its inhibition is not reversible.[79] Paclitaxel was found to be a potent and highly efficacious antimigratory agent against both coronary artery smooth muscle and endothelial cells: at higher concentrations, paclitaxel blocks cell division at mitosis, while at lower concentrations paclitaxel affects other cellular processes that can lead to an arrest in the S phase or at the G1/S interface or even lead to apoptosis.[80] Mitotic arrest induced by paclitaxel was shown to result in a large, multinucleated cell phenotype (e.g., mitotic slippage) with subsequent cell death by apoptotic mechanisms. Paclitaxel-induced apoptotic cell death could also explain the concomitant loss of medial cellularity: hence, the predominant mechanism behind paclitaxel reducing neointimal hyperplasia is cytotoxicity. Moreover, as visible from Figure 10, also high concentrations of salicylate inhibit SMC proliferation: salicylate inhibited predominantly Cdk-2 activity, whereas it had a lesser effect on Cdk-6 and no effect on Cdk-4 activity. Salycilate was shown to inhibit the proinflammatory transcription factor NF-κB23 in part by inhibiting IKK-β, one of the kinases responsible for IκB degradation. NF-κB is a member of the Rel family of transcription factors and plays an important role in the regulation of genes involved in inflammation, cell differentiation, and cell growth.[58,81]

The comparisons between experimental and calculated growth profiles (Figures 9 and 10) match experimental trends about the observed dose−dependent effect of the drug inhibitory action well. However, the same magnitude order of estimated kinetic parameters (Table 3) and the agreement between mathematical simulations and experimental data sets highlighted and confirmed the reliability of the here proposed corpuscular approach to describe SMC growth. Finally, the lumped kinetics parameters, determined to best-fit the experimental data in the last study examined, are in the range of 1 × 10^{-4} and 1 × 10^{-6} h^{-1} for the maximum growth and death rates (G and D_{max}), respectively, while a characteristic occlusion time (τ_R) of 20 days was calculated.

3.3. *In Vivo* Neointimal Thickening Inhibition. To complete our study and to estimate the restenosis characteristic time values for real *in vivo* conditions, three *in vivo* studies of different authors were examined, and regression-based simulations were thereof performed. In the first case,[57] nine domestic pigs received stainless steel stents into the left anterior descending (LAD) arteries while injecting 80 mL of iopromide containing 200 μM paclitaxel as intermittent boluses. At regular intervals after drug administration, blood samples were taken, and paclitaxel was therefrom extracted. Obtained samples were

then analyzed, using HPLC, to determine the time course of systemic paclitaxel concentration. Coronary artery segments of 1.5 cm length were analyzed 5 min, 2 h, and 24 h after catheterization to measure paclitaxel concentration (administered by intracoronary procedure) and to geometrically quantify in-stent restenosis in terms of maximal neointimal thickness and neointimal area. In particular, initial concentrations measuring 10−15 μM were comparable for all LAD segments, while two hours after stent placement, paclitaxel concentrations in the samples were about 2 μM. Moreover, in the same study, stainless steel stents were implanted into the LAD arteries in 17 domestic pigs. The animals were randomized to control (contrast agent iopromide-370): 80 mL of intracoronary iopromide plus 200 μM paclitaxel and 80 mL of intravenous iopromide plus 200 μM paclitaxel, respectively. Histologic analysis revealed that high-dose intracoronary paclitaxel led to a reduction of neointimal area by 56% and maximal neointimal thickness by 62%, while intravenous administration strategies have no inhibitory effects. These *in vivo* results well agree with data obtained from *in vitro* experiments (Figure 9), showing direct pharmacokinetic evidence in active compounds uptaking in the vessel wall of coronary arteries and adjacent tissue at paclitaxel concentrations in the 3−15 μM interval values, which is also comparable to the therapeutic window used in the *in vitro* cell assays mentioned above.

Drachman et al.[55] investigated the *in vivo* (in rabbit model) restenosis inhibition and intima tissue response (incomplete healing, few smooth muscle cells, late persistence of macrophages, and dense fibrin) of 15 stents coated with a thin layer of PLACL copolymer alone or containing paclitaxel (200 μg): the comparison between experimental data and numerical simulations is presented in Figure 11. The same figure presents also

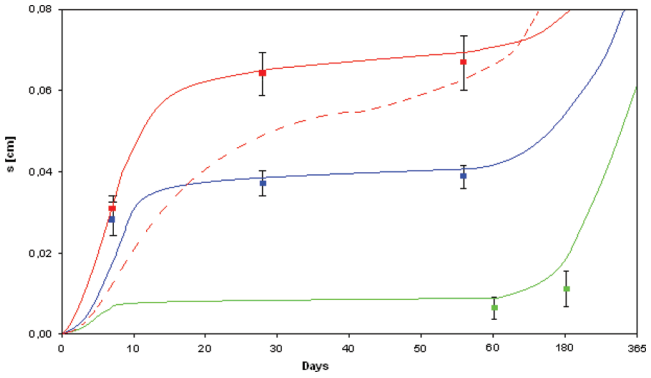

Figure 11. Comparison between the experimental and calculated neointimal thickening reduction (drug-free, paclitaxel loaded PLACL and PLGA coated DES's with s.d. = 0.007, s.d. = 0.005 and s.d. = 0.0001, red, blue, and green lines, respectively). Experimental data are taken from refs 53 and 55.

data relating to in-stent restenosis, monitored in a clinically relevant porcine coronary artery model,[53] compared to the simulated one. Drachman and co-workers showed that, by slowing paclitaxel release rate, it is possible to mitigate toxic effects while still achieving a significant attenuation of neointimal regrowth at the 30 day time point.

The lumped kinetic parameters determined to best-fit the above set of *in vivo* experimental data are comparable (in term of magnitude order) to those estimated from the *in vitro* conditions (Figure 11, continuous lines), even if scarcity of data did not allow any statistical test.

Notably, the corpuscular approach shows agreement with the experimental data, better in terms of profile than exact numerical matching (Figure 11, red dashed line): this might be due to the different experimental settings and the relatively small amount of available data sets, which often have short validation fields (<17 days) too. The decrease in SMC growth rate would be an opportunity for the endothelial lining of the artery to regrow, preventing thus further restenosis, thrombus formation, extracellular matrix production, and geometric remodeling.

3.4. Regression-Free Simulations. The few experimental data available on neointimal thickening in real *in vivo* conditions, the small number of monitoring points, as well as the large standard deviations in all *in vitro* studies considered, did not allow any statistical validation of our results in term of quantitative goodness-of-fit of models to data. Therefore, regression-free simulations were performed to highlight the system dynamic responses, in term of drug release and neointimal thickening profiles, to variations of main coating design parameters.

In particular, some simulations on drug release and neointimal thickening profiles were performed to highlight the influence of polymer composition, strongly related to coating degradation mechanisms, both on drug release and on restenosis inhibition (Figures 12 and 13). Figure 12 highlights

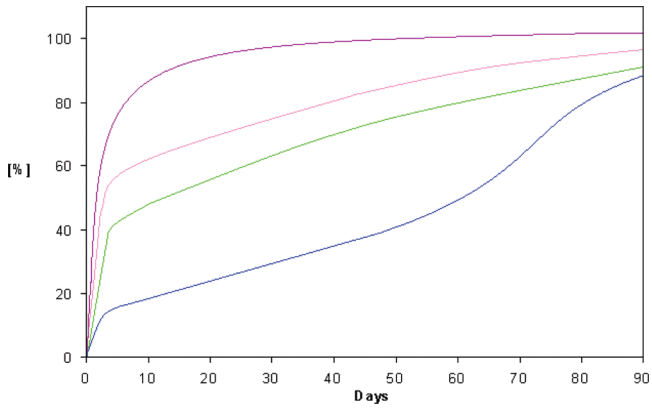

Figure 12. Simulations of paclitaxel release from lightly loaded (3% wt.) DES varying the composition of the thin (30 μm) coating (PCL, PLACL, PLLA, PLGA, violet, pink, green, and blue lines, respectively).

that only thin PLGA films can ensure a sustained drug release able to maintain drug extracellular concentrations within the therapeutic window for a long−term period (>3 months after stent implantation) well. Figure 13 shows restenosis inhibition and its dependence on polymer coating: PLGA film evidence the ability to reduce its thickening, so preserving high functionality. This consideration also agrees with recent advances and efforts in DES technology, all focused on the development of thin PLA coated DES.[16]

Finally, SMC growth profiles, by varying the extracellular drug concentration, were predicted. The simulated profiles reported in Figure 14 evidence the nonlinear dependence of cell growth on extracellular drug concentration well. For sake of completeness, the validity of these predictive extrapolations may depend also on the role played by many other phenomena, such as, for example, the effects of biological compound on degradation, bioerosion, local inflammatory response, and so

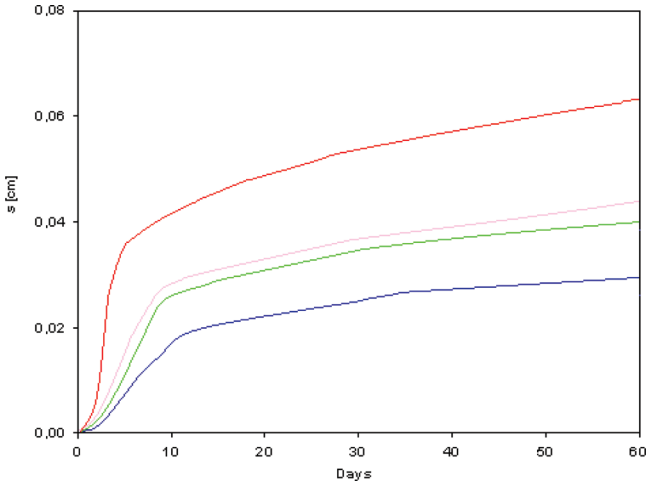

Figure 13. Comparison between predictive simulations of restenosis inhibition due to pharmaco-active drug delivery from DES, varying the composition of the thin (30 μm) coating (PLACL, PLLA, PLGA, violet, pink, green, and blue lines, respectively). The unperturbed growth curve is also reported (red line), to allow a comparison with the drug-free conditions.

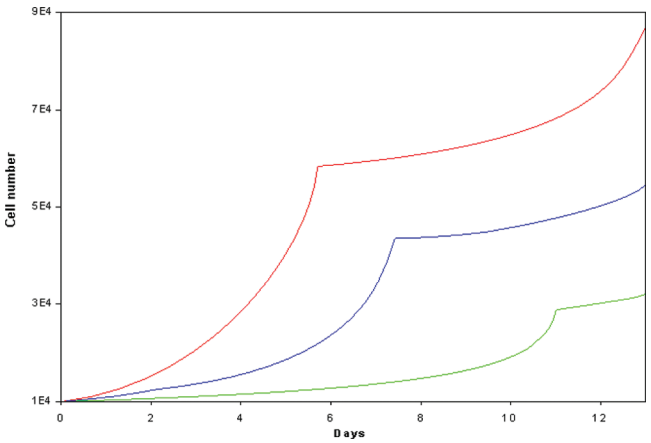

Figure 14. Predictive simulations of SMC growth inhibition varying the extracellular paclitaxel concentration (drug-free, 2.5 μM and 10 μM: red, blue, and green lines, respectively).

forth. Even if the said scarcity of experimental data did not allow to precisely consider these aspects, the model robustness was anyhow assessed: its reliability is, indeed, due to the fact that all mostly relevant phenomena are taken into consideration and described by physical sound meaning equations.

4. CONCLUSIONS

In this work, a robust mathematical model was developed, capable of taking into account polymer degradation, SMC proliferation, and drug delivery, considering that the final behavior of the stent device is the synergic result of all of these phenomena. Furthermore, the model can describe the system both for *in vitro* and *in vivo* conditions. Polymer degradation and drug delivery are described through a first principles approach by means of mass conservation equations, which contain physical sound meaning parameters such as kinetic constants and diffusion coefficients: indeed, these phenomena are not considered with classic empirical regression formulas, as often appears in literature. Model reliability, and thus the validity of the needed hypothesis to formulate the equations, was validated against various and diverse sets of experimental data taken from literature. Moreover, considering polymer degradation and drug delivery, hypotheses are based on the accepted explanation of general mechanisms that govern these phenomena. SMC proliferation equations need a quite simplified view, because of the complexity of the phenomena that intervene and the lack of knowledge about their synergic effects. In all examined cases, simulation results exhibited a satisfactory quantitative match with experimental data: this confirms the physical and biological consistency of the hypothesis and the reliability of the chosen approach.

The purpose of such modeling activity, as mentioned, is to provide a simple but powerful tool to understand the influence of design parameters on stent behavior: this also allows a smart device design, tailoring the final product according to the specific needs. Indeed, this model was developed with the idea that simplicity and ease of use should keep the pace with phenomenological understanding, but without loosing any robustness or any generality. Moreover, thanks to its simplicity and to the very low system requirements and CPU time, particularly with respect to FEM simulations, our model allows obtaining immediate views of system behavior. Hence, from an applicative point of view, it is possible to optimize the experimental activity, which can be expensive and time-consuming, through a "model driven" experimental approach, thus avoiding the classic "trial and error" *modus operandi*: a more careful management of resources is nowadays an implicit need to be fulfilled in all research and development activities.

AUTHOR INFORMATION

Corresponding Author

*Politecnico di Milano, Dipartimento di Chimica Materiali, Ingegneria Chimica, Via Mancinelli 7, Milano 20133, Italy. Tel.: +39 02 2399 3145; fax: +39 02 2399 3180; e-mail address: giuseppe.perale@polimi.it (G.P.).

Author Contributions

†These authors contributed equally to this work.

Notes

The authors declare no competing financial interest.

REFERENCES

(1) Moon, S.; Na, K.; Yang, S. G. An acetylated polysaccharide-PTFE membrane-covered stent for the delivery of gemcitabine for treatment of gastrointestinal cancer and related stenosis. *Biomaterials* **2011**, *32* (14), 3603−3610.

(2) Xi, T.; Gao, R.; Xu, B.; Chen, L.; Luo, T.; Liu, J.; Wei, Y.; Zhong, S. In vitro and in vivo changes to PLGA/sirolimus coating on drug eluting stents. *Biomaterials* **2010**, *31* (19), 5151−8.

(3) Sousa, J. E.; Costa, J. R., Jr.; Abizaid, A. 10-year follow-up of the first Cypher stent implanted in human: an invasive evaluation with angiography, intravascular ultrasound, and optical coherence tomography. *JACC Cardiovasc. Interv.* **2010**, *3* (5), 556−8.

(4) Sousa, J. E.; Serruys, P. W.; Costa, M. A. New frontiers in cardiology: drug-eluting stents: Part II. *Circulation* **2003**, *107* (18), 2383−9.

(5) Venkatraman, S.; Boey, F. Release profiles in drug-eluting stents: issues and uncertainties. *J. Controlled Release* **2007**, *120* (3), 149−60.

(6) McFadden, E. P.; Stabile, E.; Regar, E.; Cheneau, E.; Ong, A. T.; Kinnaird, T.; Suddath, W. O.; Weissman, N. J.; Torguson, R.; Kent, K. M.; Pichard, A. D.; Satler, L. F.; Waksman, R.; Serruys, P. W. Late thrombosis in drug-eluting coronary stents after discontinuation of antiplatelet therapy. *Lancet* **2004**, *364* (9444), 1519−21.

(7) Mehilli, J.; Byrne, R. A.; Tiroch, K.; Pinieck, S.; Schulz, S.; Kufner, S.; Massberg, S.; Laugwitz, K. L.; Schomig, A.; Kastrati, A. Randomized

trial of paclitaxel- versus sirolimus-eluting stents for treatment of coronary restenosis in sirolimus-eluting stents: the ISAR-DESIRE 2 (Intracoronary Stenting and Angiographic Results: Drug Eluting Stents for In-Stent Restenosis 2) study. *J. Am. Coll. Cardiol.* **2010**, *55* (24), 2710−6.
(8) Lei, L.; Guo, S. R.; Chen, W. L.; Rong, H. J.; Lu, F. Stents as a platform for drug delivery. *Expert Opin. Drug Delivery* **2011**, *8* (6), 813−31.
(9) Tesfamariam, B. Drug release kinetics from stent device-based delivery systems. *J. Cardiovasc. Pharmacol.* **2008**, *51* (2), 118−25.
(10) Raval, A.; Parikh, J.; Engineer, C. Mechanism and in Vitro Release Kinetic Study of Sirolimus from a Biodegradable Polymeric Matrix Coated Cardiovascular Stent. *Ind. Eng. Chem. Res.* **2011**, *50* (16), 9539−9549.
(11) Lockwood, N. A.; Hergenrother, R. W.; Patrick, L. M.; Stucke, S. M.; Steendam, R.; Pacheco, E.; Virmani, R.; Kolodgie, F. D.; Hubbard, B. In vitro and in vivo characterization of novel biodegradable polymers for application as drug-eluting stent coatings. *J. Biomater. Sci., Polym. Ed.* **2010**, *21* (4), 529−52.
(12) Cohen-Sela, E.; Chorny, M.; Koroukhov, N.; Danenberg, H. D.; Golomb, G. A new double emulsion solvent diffusion technique for encapsulating hydrophilic molecules in PLGA nanoparticles. *J. Controlled Release* **2009**, *133* (2), 90−5.
(13) Danenberg, H. D.; Golomb, G.; Groothuis, A.; Gao, J.; Epstein, H.; Swaminathan, R. V.; Seifert, P.; Edelman, E. R. Liposomal alendronate inhibits systemic innate immunity and reduces in-stent neointimal hyperplasia in rabbits. *Circulation* **2003**, *108* (22), 2798−804.
(14) Cohen-Sela, E.; Rosenzweig, O.; Gao, J.; Epstein, H.; Gati, I.; Reich, R.; Danenberg, H. D.; Golomb, G. Alendronate-loaded nanoparticles deplete monocytes and attenuate restenosis. *J. Controlled Release* **2006**, *113* (1), 23−30.
(15) Haber, E.; Afergan, E.; Epstein, H.; Gutman, D.; Koroukhov, N.; Ben-David, M.; Schachter, M.; Golomb, G. Route of administration-dependent anti-inflammatory effect of liposomal alendronate. *J. Controlled Release* **2010**, *148* (2), 226−33.
(16) Grube, E.; Buellesfeld, L. BioMatrix Biolimus A9-eluting coronary stent: a next-generation drug-eluting stent for coronary artery disease. *Expert Rev. Med. Device* **2006**, *3* (6), 731−41.
(17) Tamai, H.; Igaki, K.; Kyo, E.; Kosuga, K.; Kawashima, A.; Matsui, S.; Komori, H.; Tsuji, T.; Motohara, S.; Uehata, H. Initial and 6-month results of biodegradable poly-l-lactic acid coronary stents in humans. *Circulation* **2000**, *102* (4), 399−404.
(18) Ma, X.; Oyamada, S.; Wu, T.; Robich, M. P.; Wu, H.; Wang, X.; Buchholz, B.; McCarthy, S.; Bianchi, C. F.; Sellke, F. W.; Laham, R. In vitro and in vivo degradation of poly(D,L-lactide-co-glycolide)/amorphous calcium phosphate copolymer coated on metal stents. *J. Biomed. Mater. Res., Part A* **2011**, *96* (4), 632−8.
(19) Li, Y.; Bhindi, R.; Khachigian, L. M. Recent developments in drug-eluting stents. *J. Mol. Med.* **2011**, *89* (6), 545−53.
(20) Acharya, G.; Park, K. Mechanisms of controlled drug release from drug-eluting stents. *Adv. Drug Delivery Rev.* **2006**, *58* (3), 387−401.
(21) Sung, H. J.; Meredith, C.; Johnson, C.; Galis, Z. S. The effect of scaffold degradation rate on three-dimensional cell growth and angiogenesis. *Biomaterials* **2004**, *25* (26), 5735−5742.
(22) Scapin, S. M. N.; Silva, D. R. M.; Joazeiro, P. P.; Alberto-Rincon, M. C.; Luciano, R. M.; Duek, E. A. R. Use of triethylcitrate plasticizer in the production of poly-L-lactic acid implants with different degradation times. *J. Mater. Sci.: Mater. Med.* **2003**, *14* (7), 635−640.
(23) Unger, F.; Westedt, U.; Hanefeld, P.; Wombacher, R.; Zimmermann, S.; Greiner, A.; Ausborn, M.; Kissel, T. Poly(ethylene carbonate): a thermoelastic and biodegradable biomaterial for drug eluting stent coatings? *J. Controlled Release* **2007**, *117* (3), 312−21.
(24) van der Hoeven, B. L.; Pires, N. M.; Warda, H. M.; Oemrawsingh, P. V.; van Vlijmen, B. J.; Quax, P. H.; Schalij, M. J.; van der Wall, E. E.; Jukema, J. W. Drug-eluting stents: results, promises and problems. *Int. J. Cardiol.* **2005**, *99* (1), 9−17.
(25) Virmani, R.; Farb, A.; Guagliumi, G.; Kolodgie, F. D. Drug-eluting stents: caution and concerns for long-term outcome. *Coronary Artery Dis.* **2004**, *15* (6), 313−318.
(26) Stone, G. W.; Ellis, S. G.; Cannon, L.; Mann, J. T.; Greenberg, J. D.; Spriggs, D.; O'Shaughnessy, C. D.; DeMaio, S.; Hall, P.; Popma, J. J.; Koglin, J.; Russell, M. E.; Investigators, T. V. Comparison of a polymer-based paclitaxel-eluting stent with a bare metal stent in patients with complex coronary artery disease - A randomized controlled trial. *J. Am. Med. Assoc.* **2005**, *294* (10), 1215−1223.
(27) Han, D. W.; Jung, D. Y.; Park, J. C.; Cho, H. H.; Hyon, S. H.; Han, D. K. Underlying mechanism for suppression of vascular smooth muscle cells by green tea polyphenol EGCG released from biodegradable polymers for stent application. *J. Biomed. Mater. Res., Part A* **2010**, *95* (2), 424−33.
(28) Dzau, V. J.; Braun-Dullaeus, R. C.; Sedding, D. G. Vascular proliferation and atherosclerosis: new perspectives and therapeutic strategies. *Nat. Med.* **2002**, *8* (11), 1249−56.
(29) Levin, A. D.; Vukmirovic, N.; Hwang, C. W.; Edelman, E. R. Specific binding to intracellular proteins determines arterial transport properties for rapamycin and paclitaxel. *Proc. Natl. Acad. Sci. U.S.A.* **2004**, *101* (25), 9463−7.
(30) Martin, D.; Boyle, F. J. Computational structural modelling of coronary stent deployment: a review. *Comput. Methods Biomech.* **2011**, *14* (4), 331−348.
(31) Hossainy, S.; Prabhu, S. A mathematical model for predicting drug release from a biodurable drug-eluting stent coating. *J. Biomed. Mater. Res., Part A* **2008**, *87* (2), 487−93.
(32) Yang, C. M.; Burt, H. A. Drug-eluting stents: Factors governing local pharmacokinetics. *Adv. Drug Delivery Rev.* **2006**, *58* (3), 402−411.
(33) Kiousis, D. E.; Gasser, T. C.; Holzapfel, G. A. A numerical model to study the interaction of vascular stents with human atherosclerotic lesions. *Ann. Biomed. Eng.* **2007**, *35* (11), 1857−1869.
(34) Zahedmanesh, H.; Lally, C. Determination of the influence of stent strut thickness using the finite element method: implications for vascular injury and in-stent restenosis. *Med. Biol. Eng. Comput.* **2009**, *47* (4), 385−393.
(35) Zhao, H. Q.; Jayasinghe, D.; Hossainy, S.; Schwartz, L. B. A theoretical model to characterize the drug release behavior of drug-eluting stents with durable polymer matrix coating. *J. Biomed. Mater. Res., Part A* **2012**, *100A* (1), 120−124.
(36) Vergara, C.; Zunino, P. Multiscale Boundary Conditions for Drug Release from Cardiovascular Stents. *Multiscale Model Simul.* **2008**, *7* (2), 565−588.
(37) Seidlitz, A.; Nagel, S.; Semmling, B.; Grabow, N.; Martin, H.; Senz, V.; Harder, C.; Sternberg, K.; Schmitz, K. P.; Kroemer, H. K.; Weitschies, W. Examination of drug release and distribution from drug-eluting stents with a vessel-simulating flow-through cell. *Eur. J. Pharm. Biopharm.* **2011**, *78* (1), 36−48.
(38) Formaggia, L.; Minisini, S.; Zunino, P. Modeling Polymeric Controlled Drug Release and Transport Phenomena in the Arterial Tissue. *Math. Mod. Methods Appl. Sci.* **2010**, *20* (10), 1759−1786.
(39) D'Angelo, C.; Zunino, P.; Porpora, A.; Morlacchi, S.; Migliavacca, F. Model Reduction Strategies Enable Computational Analysis of Controlled Drug Release from Cardiovascular Stents. *Siam J. Appl. Math.* **2011**, *71* (6), 2312−2333.
(40) D'Angelo, C.; Zunino, P. A Numerical Study of the Interaction of Blood Flow and Drug Release from Cardiovascular Stents. *Numer. Math. Adv. Appl.* **2008**, 75−82.
(41) Kagadis, G. C.; Skouras, E. D.; Bourantas, G. C.; Paraskeva, C. A.; Katsanos, K.; Karnabatidis, D.; Nikiforidis, G. C. Computational representation and hemodynamic characterization of in vivo acquired severe stenotic renal artery geometries using turbulence modeling. *Med. Eng. Phys.* **2008**, *30* (5), 647−660.
(42) Kolachalama, V. B.; Tzafriri, A. R.; Arifin, D. Y.; Edelman, E. R. Luminal flow patterns dictate arterial drug deposition in stent-based delivery. *J. Controlled Release* **2009**, *133* (1), 24−30.
(43) Balakrishnan, B.; Dooley, J. F.; Kopia, G.; Edelman, E. R. Intravascular drug release kinetics dictate arterial drug deposition,

retention, and distribution. *J. Controlled Release* **2007**, *123* (2), 100−108.
(44) Borghi, A.; Foa, E.; Balossino, R.; Migliavacca, F.; Dubini, G. Modelling drug elution from stents: effects of reversible binding in the vascular wall and degradable polymeric matrix. *Comput. Methods Biomech.* **2008**, *11* (4), 367−377.
(45) Prabhu, S.; Hossainy, S. Modeling of degradation and drug release from a biodegradable stent coating. *J. Biomed. Mater. Res., Part A* **2007**, *80A* (3), 732−741.
(46) Tambaca, J.; Kosor, M.; Canic, S.; Paniagua, D. Mathematical Modeling of Vascular Stents. *Siam J. Appl. Math.* **2010**, *70* (6), 1922−1952.
(47) Morlacchi, S.; Keller, B.; Arcangeli, P.; Balzan, M.; Migliavacca, F.; Dubini, G.; Gunn, J.; Arnold, N.; Narracott, A.; Evans, D.; Lawford, P. Hemodynamics and In-stent Restenosis: Micro-CT Images, Histology, and Computer Simulations. *Ann. Biomed. Eng.* **2011**, *39* (10), 2615−2626.
(48) Pant, S.; Bressloff, N. W.; Limbert, G. Geometry parameterization and multidisciplinary constrained optimization of coronary stents. *Biomech. Model Mech.* **2012**, *11* (1−2), 61−82.
(49) Muliana, A.; Rajagopal, K. R. Modeling the response of nonlinear viscoelastic biodegradable polymeric stents. *Int. J. Solids Struct.* **2012**, *49* (7−8), 989−1000.
(50) Lu, L.; Garcia, C. A.; Mikos, A. G. In vitro degradation of thin poly(DL-lactic-co-glycolic acid) films. *J. Biomed. Mater. Res.* **1999**, *46* (2), 236−44.
(51) Lao, L. L.; Venkatraman, S. S. Paclitaxel release from single and double-layered poly(DL-lactide-co-glycolide)/poly(L-lactide) film for biodegradable coronary stent application. *J. Biomed. Mater. Res., Part A* **2008**, *87* (1), 1−7.
(52) Pan, C. J.; Tang, J. J.; Weng, Y. J.; Wang, J.; Huang, N. Preparation and characterization of rapamycin-loaded PLGA coating stent. *J. Mater. Sci.: Mater. Med.* **2007**, *18* (11), 2193−8.
(53) Jabara, R.; Chronos, N.; Tondato, F.; Conway, D.; Molema, W.; Park, K.; Mabin, T.; King, S.; Robinson, K. Toxic vessel reaction to an absorbable polymer-based paclitaxel-eluting stent in pig coronary arteries. *J. Invasive Cardiol.* **2006**, *18* (8), 383−90.
(54) Lao, L. L.; Venkatraman, S. S. Adjustable paclitaxel release kinetics and its efficacy to inhibit smooth muscle cells proliferation. *J. Controlled Release* **2008**, *130* (1), 9−14.
(55) Drachman, D. E.; Edelman, E. R.; Seifert, P.; Groothuis, A. R.; Bornstein, D. A.; Kamath, K. R.; Palasis, M.; Yang, D.; Nott, S. H.; Rogers, C. Neointimal thickening after stent delivery of paclitaxel: change in composition and arrest of growth over six months. *J. Am. Coll. Cardiol.* **2000**, *36* (7), 2325−32.
(56) Tan, L. P.; Venkatraman, S. S.; Sung, P. F.; Wang, X. T. Effect of plasticization on heparin release from biodegradable matrices. *Int. J. Pharm.* **2004**, *283* (1−2), 89−96.
(57) Scheller, B.; Speck, U.; Schmitt, A.; Bohm, M.; Nickenig, G. Addition of paclitaxel to contrast media prevents restenosis after coronary stent implantation. *J. Am. Coll. Cardiol.* **2003**, *42* (8), 1415−20.
(58) Marra, D. E.; Simoncini, T.; Liao, J. K. Inhibition of vascular smooth muscle cell proliferation by sodium salicylate mediated by upregulation of p21(Waf1) and p27(Kip1). *Circulation* **2000**, *102* (17), 2124−30.
(59) Pitt, G. C. *Biodegradable Polymers and Plastic*; Royal Society of Chemistry: London, U.K., 1992.
(60) Arosio, P.; Busini, V.; Perale, G.; Moscatelli, D.; Masi, M. A new model of resorbable device degradation and drug release - part I: zero order model. *Polym. Int.* **2008**, *57* (7), 912−920.
(61) Perale, G.; Arosio, P.; Moscatelli, D.; Barri, V.; Muller, M.; Maccagnan, S.; Masi, M. A new model of resorbable device degradation and drug release: transient 1-dimension diffusional model. *J. Controlled Release* **2009**, *136* (3), 196−205.
(62) Grizzi, I.; Garreau, H.; Li, S.; Vert, M. Hydrolytic Degradation of Devices Based on Poly(Dl-Lactic Acid) Size-Dependence. *Biomaterials* **1995**, *16* (4), 305−311.
(63) von Burkersroda, F.; Schedl, L.; Gopferich, A. Why degradable polymers undergo surface erosion or bulk erosion. *Biomaterials* **2002**, *23* (21), 4221−4231.
(64) Alexis, F. Factors affecting the degradation and drug-release mechanism of poly(lactic acid) and poly[(lactic acid)-co-(glycolic acid)]. *Polym. Int.* **2005**, *54* (1), 36−46.
(65) Tsuji, H.; Tezuka, Y. Alkaline and enzymatic degradation of L-lactide copolymers, 1 - Amorphous-made films of L-lactide copolymers with D-lactide, glycolide, and epsilon-caprolactone. *Macromol. Biosci.* **2004**, *5* (2), 135−148.
(66) Tsuji, H.; Tezuka, Y.; Yamada, K. Alkaline and enzymatic degradation of L-lactide copolymers. II. Crystallized films of poly(L-lactide-co-D-lactide) and poly(L-lactide) with similar crystallinities. *J. Polym. Sci., Part B: Polym. Phys.* **2005**, *43* (9), 1064−1075.
(67) Numata, K.; Finne-Wistrand, A.; Albertsson, A. C.; Doi, Y.; Abe, H. Enzymatic degradation of monolayer for poly(lactide) revealed by real-time atomic force microscopy: Effects of stereochemical structure, molecular weight, and molecular branches on hydrolysis rates. *Biomacromolecules* **2008**, *9* (8), 2180−2185.
(68) Zhao, Z. X.; Yang, L.; Hu, Y. F.; He, Y.; Wei, J.; Li, S. M. Enzymatic degradation of block copolymers obtained by sequential ring opening polymerization of L-lactide and epsilon-caprolactone. *Polym. Degrad. Stab.* **2007**, *92* (10), 1769−1777.
(69) Holy, C. E.; Dang, S. M.; Davies, J. E.; Shoichet, M. S. In vitro degradation of a novel poly(lactide-co-glycolide) 75/25 foam. *Biomaterials* **1999**, *20* (13), 1177−1185.
(70) Busini, V.; Arosio, P.; Masi, M. Mechanistic modelling of avascular tumor growth and pharmacokinetics influence - Part I. *Chem. Eng. Sci.* **2007**, *62* (7), 1877−1886.
(71) Masaro, L.; Zhu, X. X. Physical models of diffusion for polymer solutions, gels and solids. *Prog. Polym. Sci.* **1999**, *24* (5), 731−775.
(72) Vrentas, J. S.; Vrentas, C. M. Diffusion in glassy polymers. *J. Polym. Sci., Part B: Polym. Phys.* **2003**, *41* (8), 785−788.
(73) Liggins, R. T.; Hunter, W. L.; Burt, H. M. Solid-state characterization of paclitaxel. *J. Pharm. Sci.* **1997**, *86* (12), 1458−63.
(74) Simamora, P.; Alvarez, J. M.; Yalkowsky, S. H. Solubilization of rapamycin. *Int. J. Pharm.* **2001**, *213* (1−2), 25−9.
(75) Kerns, E. H.; Hill, S. E.; Detlefsen, D. J.; Volk, K. J.; Long, B. H.; Carboni, J.; Lee, M. S. Cellular uptake profile of paclitaxel using liquid chromatography tandem mass spectrometry. *Rapid Commun. Mass Spectrom.* **1998**, *12* (10), 620−4.
(76) Gopferich, A. Mechanisms of polymer degradation and erosion. *Biomaterials* **1996**, *17* (2), 103−14.
(77) Casalini, T.; Masi, M.; Perale, G. Drug eluting sutures: a model for in vivo estimations. *Int. J. Pharm.* **2012**, *429* (1), 148−157.
(78) Powell, R. J.; Cronenwett, J. L.; Fillinger, M. F.; Wagner, R. J. Effect of endothelial cells and transforming growth factor-beta 1 on cultured vascular smooth muscle cell growth patterns. *J. Vasc. Surg.* **1994**, *20* (5), 787−94.
(79) Parry, T. J.; Brosius, R.; Thyagarajan, R.; Carter, D.; Argentieri, D.; Falotico, R.; Siekierka, J. Drug-eluting stents: Sirolimus and paclitaxel differentially affect cultured cells and injured arteries. *Eur. J. Pharmacol.* **2005**, *524* (1−3), 19−29.
(80) Giannakakou, P.; Robey, R.; Fojo, T.; Blagosklonny, M. V. Low concentrations of paclitaxel induce cell type-dependent p53, p21 and G1/G2 arrest instead of mitotic arrest: molecular determinants of paclitaxel-induced cytotoxicity. *Oncogene* **2001**, *20* (29), 3806−3813.
(81) Yin, M. J.; Yamamoto, Y.; Gaynor, R. B. The anti-inflammatory agents aspirin and salicylate inhibit the activity of I kappa B kinase-beta. *Nature* **1998**, *396* (6706), 77−80.